Tech : Journal of Engineering Science
Vol. 2, No. 1, 2026.
e-ISSN: 3109-7790 (online)
https://jurnal.sinesia.id/index.php/tech/index

Enhancing the Stability Characteristics of the Compliant Vertical Access Riser Using the Effects of Riser Damping and Axial Tension

Tochukwu Chukwuka Oraelosi[1], Solomon Chukwuka Nwigbo[1], Sunday Madubueze Ofochebe[1], Obiora B. Ezeudu[2]
Correspondence Email : sm.ofochebe@unizik.edu.ng
[1]Department of Mechanical Engineering, Nnamdi Azikiwe University, Awka, Nigeria
[2]Department of Civil Engineering, University of Victoria, British Columbia, Canada

Info Article
|Submitted: 18 February 2026 **|Revised**: 8 March 2026 **|Accepted**: 8 March 2026
|Published: 10 March 2026
How to Cite : Tochukwu Chukwuka Oraelosi, etc., "Enhancing the Stability Characteristics of the Compliant Vertical Access Riser Using the Effects of Riser Damping and Axial Tension", *Tech : Journal of Engineering Scince*, Vol. 2, No. 1, 2026, P. 83-101.

ABSTRACT

In this paper, practical ways to enhance the stability characteristics and vibration response of the compliant vertical access riser (CVAR) system are studied. The CVAR system is proposed for a floating production system operating in water field of nominal depth 2438m. The study utilized a state-space model of the riser motion developed from semi-discretization of the governing equation of motion by Galerkin's method. The stability analysis proceeds from a desirable static state of the riser system found in literature. Performance of the CVAR system under mode-coupling condition is studied exclusively, to account for the effects of damping and axial tension. The study found that the stability of the CVAR system is improved when the axial tension or the damping is increased, however, the level of improvement achievable through independent adjustment of these variables is limited and short of the field requirement. To achieve a sustainable stability for a CVAR system operated under adverse weather condition, the combined effects of increased riser damping and tension could be utilized. In the present case, about 100% increase in axial tension, from the static equilibrium condition, is required of the CVAR system with damping coefficient of 0.5, to increase the minimum critical platform heave amplitude from a nominal value $\leq 0.5m$ *to a desirable value* $\geq 2m$*, over the excitation frequency range.*

Keywords: *Stability characteristics, compliant vertical access, riser, effects of riser damping, axial tension*

Introduction

Hydrocarbons (oil, gas, and coal) continue to dominate the global energy mix, accounting for approximately 80–82% of total primary energy consumption (American Oil and Gas Reporter, 2025). In spite of the recent campaign for alternative renewable and eco-friendly energy sources, major producers of hydrocarbon are not discouraged from production, instead they are driving research towards production of cleaner energy from hydrocarbon, that has less negative impact on the environment (Ağbulut & Sarıdemir, 2021;Zhu, 2019). Much focus of the exploration of hydrocarbons has been on oil and natural gas. Almost all the land-based oil and gas sources have been discovered and, at the current rate of consumption, they would be depleted in a near future time. So, it brings renewed hope for sustainability to discover that beneath the seabed lies vast quantities of oil and gas reserves. Since the last century, exploration has continued to shift from onshore (shallow water) to deep water offshore locations with current depths

exceeding 3,000 metres (Zuoqian et al., 2022; Zhixin et al., 2023; C et al., 2024). The shift to deeper waters has come with serious challenges on technology. One of the most important technological equipment required in offshore operations is the marine risers. Risers are needed to support both exploration (Woo et al., 2016) and production activities. In the exploration phase, the risers help to guide the drill string and serves as a return path for the mud(Liu et al., 2020). In the production phase, the riser system is the only transport path from the seabed through which the hydrocarbon is conveyed to the storage facilities on the production platform at the ocean surface and from there to the offload tankers or the pipelines.

The most common production riser concepts for offshore development are Top Tensioned Riser (TTR), Flexible Riser (FR), Steel Catenary Riser (SCR), Lazy Wave Riser (LWR), Hybrid Riser (HR) and Buoyancy Supported Riser (BSR) (Khan et al., 2011;Bai & Bai, 2019; Bakis & Srinil, 2019). The depth of the seabed and the prevailing environmental condition play a key role in selection of the appropriate riser concept for a particular well development. As the depth of the seabed increases towards ultradeep locations above 1500 metres, application of rigid production platforms and the compatible riser concepts such as TTRs becomes impracticable. Moreover, for reasons related to rising tension, increased hydrodynamic pressure and fatigue loading at greater water depths, other non-buoyant riser configurations such as the Steel Catenary Riser (SCR) equally become less feasible. The Floating Production System (FPS) is a preferred production platform for deepwater field operations (Wu et al. 2019; Lei & Zheng, 2016).

Currently, SCRs, LWRs, FRs and HRs are used to meet the requirements of deep-water FPS. The SCR has been successfully deployed for hydrocarbon transport in water depths exceeding 900 meters and can be considered for greater depths with modification to higher strength alloys and the use of buoyancy supporting jackets that may help to alleviate the large tensile forces generated proportionally to riser length (Buberg, 2014). The SCR and LWR systems are self-compliant, much like a flexible riser. They do not need heave compensation equipment. Flexible pipe application features include water depths above 2,000 meters, high pressure up to 70MPa, and high temperature above 65°C, as well as the ability to withstand large vessel motion in adverse weather conditions (Gonzalez et al., 2015). Extension of these conventional risers for ultra-deep-water operations is uniquely challenged by the inherent operational and economic disadvantages. The SCR is characterised by lengthy touch down and high hang-off tension which dispose it to fatigue and disengagement from thread failure by heave motion of the FPS. The LWR requires extremely high offset distance of the anchor point from the wellhead, resulting in excessively high riser overlength and uncontrollable hang-off tension.

The connective joints of HRs are complex and very problematic to use with the anchor system. Flexible risers are basically not suitable for use in high temperature and high-pressure fields due to their type of material which is of relatively low thermal resistance and low mechanical strength. Also, the production cost of large diameter flexible risers is prohibitively high for great depths (Elosta et al. 2013). Due to these shortcomings identified with the conventional production risers, the *Compliant Vertical Access Riser (CVAR)* system has been developed to increase market competitiveness and guarantee safe production at ultradeep water field. The CVAR has differentiated geometry which allows it to compensate for the motion of the platform while maintaining a vertical connection to the wellhead. This feature also allows for well interventions to be carried out directly from the production platform, thus providing some operational advantages and cost reduction (Lou, Li, et al., 2019; Li et al., 2021;Liang et al., 2023).

The idea of improving the stability characteristics/vibration response of marine risers through adjusting the riser damping or the tension has been introduced in literature. The effects of damping and mode-coupling on stability of the CVAR system have been reported by Lou, Hu, et al. (2019). This relevant article reported that (i) stability of the CVAR can be improved by increasing its damping capacity (ii) the critical level of excitation beyond which adjusting the riser damping alone cannot guarantee absolute stability of the CVAR system operated under mode coupling condition is considerably low, suggesting that in a blustery marine condition, the performance of the CVAR system may be short of the field requirement. Hence, further research is needed in this line to explore possible means to achieve a sustainable stability for the CVAR system, and enhance its dynamic performance. In response a comprehensive analysis of the combined effects of the riser damping, the hang-off tension, and the excitation parameters (including the platform heave amplitude and the platform heave frequency) on the stability characteristics and vibration response of the CVAR system is carried out in the present study. The current research is intended to provide a knowledge base for development of a CVAR system with a sustainable dynamic stability.

2. Theoretical formulations

2.1 Equation of motion

Considering the symmetry of the riser cross-section about the vertical planes, the equation of motion can be derived independently for each plane. Figure 1 shows a differential element of vertical length, dz in y-z plane. At both ends of the segment, the forces acting on the differential element are shown. These include the shear force, Q, the moment, M, and axial forces, T. The resultant of all the external loads

$f(z,t)$, inertia forces $f_1(z,t)$ and the damping forces $f_D(z,t)$ are shown at the sides of the segment.

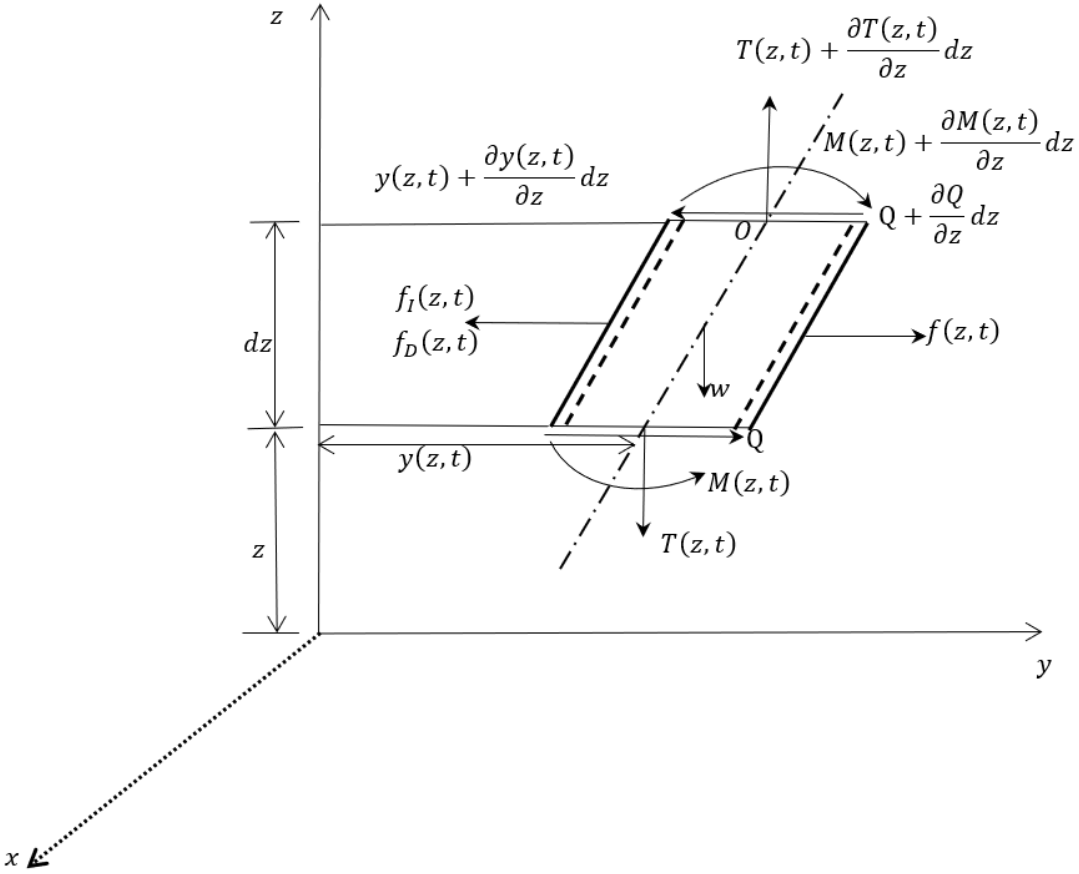

Figure 1: Free body diagram of a differential beam element

Summing the forces acting on the differential element in the horizontal plane yields

$$\frac{\partial Q}{\partial z}dz = f(z,t) - f_I(z,t) - f_D(z,t) \qquad (1)$$

where, $f_D(z,t)$ represents water resistance associated with damping parameter $c(z,t)$ and $f_I(z,t)$ is the inertia force

Summing moments about the top edge (O) we have

$$\mathrm{Q}dz = -T(z,t)\frac{\partial y(z,t)}{\partial z}dz + \frac{\partial M(z,t)}{\partial z}dz \qquad (2)$$

From moment-curvature relation for constant bending stiffness, EI

$$M(z,t) = EI\frac{\partial^2 y(z,t)}{\partial z^2} \qquad (3)$$

Differentiating equation (2) with respect to z gives

$$\frac{\partial Q}{\partial z}dz = \frac{\partial^2 M(z,t)}{\partial z^2}dz - T(z,t)\frac{\partial^2 y(z,t)}{\partial z^2}dz - \frac{\partial T(z,t)}{\partial z}\frac{\partial y(z,t)}{\partial z}dz \qquad (4)$$

Combining equations (1), (3) and (4), we have

$$EI\frac{\partial^4 y(z,t)}{\partial z^4}dz - T(z,t)\frac{\partial^2 y(z,t)}{\partial z^2}dz - \frac{\partial T(z,t)}{\partial z}\frac{\partial y(z,t)}{\partial z}dz + f_I(z,t) + f_D(z,t) = f(z,t) \quad (5)$$

If we define the inertia force $f_I(z,t)$ and the damping force $f_D(z,t)$ as follows

$$f_I(z,t) = \frac{\partial}{\partial t}\left[m(z,t)\frac{\partial y(z,t)}{\partial t}\right] \quad (6)$$

and

$$f_D(z,t) = c(z,t)\frac{\partial y(z,t)}{\partial t} \quad (7)$$

where $m(z,t)$ and $c(z,t)$ mass and damping coefficient obtained for a unit length of riser. $m(z,t)$ can be assumed to be constant over each differential element.

Then, substituting for $f_I(z,t)$ and $f_D(z,t)$ in (5) and simplifying gives the governing equation of motion of the riser as

$$EI\frac{\partial^4 y(z,t)}{\partial z^4} - \frac{\partial}{\partial z}\left[T(z,t)\frac{\partial y(z,t)}{\partial z}\right] + \bar{m}\frac{\partial^2 y(z,t)}{\partial t^2} + c(z,t)\frac{\partial y(z,t)}{\partial t} = f_z(z,t) \quad (8)$$

where the resultant external force acting on the riser per unit length denoted by $f_z(z,t)$ includes forces due to gravity f_g, buoyancy f_b, internal fluid f_i, drag from external current f_d, added mass effect f_A and vortex-induced lift force f_L; $T(z,t)$ is the effective tension, reflecting the coupling of parametric excitation and structural response:

$$T(z,t) = T(z) + T(t) \quad (9)$$

$T(z)$ is the static component of the effective tension given by

$$T(z) = T_t - wz \quad (10)$$

in which T_t is the applied tension at the top of the riser; w is the weight per unit length of the riser immersed in water; and $T(t)$is the dynamic component of the effective tension (i.e., the tension in the riser over time due to the heave motion of the platform), given by

$$T(t) = \kappa a cos(\Omega t) \quad (11)$$

where κ is coefficient of tension transfer; a is the amplitude of platform heave; and Ω is the frequency of platform heave. a and Ω are considered as the excitation parameters of the riser. $f_z(z,t)$ is the external force per unit length acting on the riser; $y(z,t)$ is the dynamic lateral displacement of the riser; z is the vertical coordinate along the riser; t is the time; E is the elastic modulus; I is the cross-sectional moment of inertia of the riser given by;

$$I = \frac{\pi}{64}(D^4 - d^4) \quad (12)$$

where D is the outside diameter and d is the inside diameter of the riser

The fourth-order partial differential equation (8) governs the riser response to a general dynamic and distributed external excitation $f_z(z,t)$. For the stability

analysis, we assume natural excitation and ignore external forcing function, i.e. $f_z(z,t) = 0$. The governing equation reduces to:

$$EI\frac{\partial^4 y(z,t)}{\partial z^4} - \frac{\partial}{\partial z}\left[T(z,t)\frac{\partial y(z,t)}{\partial z}\right] + \bar{m}\frac{\partial^2 y(z,t)}{\partial t^2} + c(z,t)\frac{\partial y(z,t)}{\partial t} = 0 \quad (13)$$

2.2 Galerkin's Method

To discretize the governing equation (13) along the spatial coordinate, y, using the Galerkin method, the general solution can be expressed in the form:

$$y(z,t) = \sum_{i=1}^{\infty} N_i(z) q_j(t) \quad (14)$$

where

$$N_i(z) = A\,sin\left(\frac{n\pi}{L}z\right) \quad (15)$$

is the mode shape function, or displacement amplitude of the ith normal mode; i is the mode order, $q_i(t)$ is a time function and L is the riser length. $'A'$ can be evaluated from the end conditions.

Making substitution for $y(z,t)$ in equation (13), we have:

$$EI\frac{\partial^4 N_i(z)}{\partial z^4}q_i(t) - T(z)\frac{\partial^2 N_i(z)}{\partial z^2}q_i(t) - T(t)\frac{\partial^2 N_i(z)}{\partial z^2}q_i(t) + \bar{m}N_i(z)\frac{\partial^2 q_i(t)}{\partial t^2} + c(z,t)N_i(z)\frac{\partial q_i(t)}{\partial t} = 0 \quad (15)$$

Further substitution for $N_i(z)$, $(i = 1,2,3,\dots,n)$ and their derivatives in equation (15), adopting the 'dot' notation for a derivative with respect to time, we have

$$\ddot{q}_i + \omega_i^2 q_i - \frac{\kappa a cos(\Omega t)}{\bar{m}}\sum_i f_{ij}\,q_i + c(z,t)\dot{q}_\iota = 0; (i = 1,2,3,\dots.,N) \quad (16)$$

The mode coupling coefficient, f_{ij} is defined as:

$$f_{ij} = \frac{\int_0^L N_i \frac{\partial^2 N_j}{\partial z^2}dz}{\int_0^L N_i^2 dz} = \begin{cases} -\dfrac{j^2\pi^2}{L^2} & i = j \\ \pm\dfrac{j^3\pi^2}{2iL^2} & i \neq j, \end{cases} \quad (17)$$

Considering the self-weight of the riser and the damping forces, the axial tension is considered to vary linearly over the riser length; such that $T(z) = T - wz$. From Vandiver theory, the natural frequency of the riser with its tension varying over the length is given as: (Vandiver and Li 2005)

$$\int_0^L \sqrt{\sqrt{\left(\frac{T(z)}{2EI}\right)^2 + \frac{\bar{m}\omega_n^2}{EI}} - \frac{T(z)}{2EI}}\,dz = n\pi \quad (18)$$

Evaluating the definite integral, we have:

$$\left[\frac{a_1 + a_2\sqrt{a_3 + b\omega_i^2} - 2b\omega_i^2}{\sqrt[3]{a_4 - \sqrt{a_3 + b\omega_i^2}}}\right] - \left[\frac{b_1 + b_2\sqrt{b_3 + b\omega_i^2} - 2b\omega_i^2}{\sqrt[3]{b_4 - \sqrt{b_3 + b\omega_i^2}}}\right] = -i\pi aw \quad (19)$$

where: $a = 1/2EI\,;\ b = \bar{m}/EI\,;\ a_1 = 2a^2(T - wL)^2; a_2 = -2a(T - wL);\ a_3 = a^2(T - wL)^2; a_4 = a(T - wL)\,;\ b_1 = 2a^2T^2; b_2 = -2aT;\ b_3 = a^2T^2; b_4 = aT$

Equation (19) yields ω_i at distributed axial tension.

Due to the self-weight of the riser, the tension in the riser decreases with water depth. This results in multi-mode vibration and mode coupling/interference at parametric excitation conditions.

The nonlinear damping per unit length, $c(z,t)$ can be expressed in this case using the linearized Morison's equation described as: (Lou et al. 2019;Wu et al., 2019):

$$f_{drag} = \frac{1}{2}\rho D C_d \sum_{j=1}^{N}\left[N_i(z)\dot{q}_i(t)\alpha_i N_{i,max}\omega_i\right] = c(z,t)\dot{q}_\iota \quad (20)$$

where C_d is drag coefficient, $N_{i,max}$ is the peak value of displacement amplitude and α_i is a coefficient which depends on the displacement mode defined by: (Lou et al. 2019)

$$\alpha_i = \frac{1}{\omega_i N_{i,max}} \frac{\int_{t=0}^{2\pi/\omega_i}\int_{z=0}^{L}\{N_i(z)\dot{q}_i(t)\}^2|N_i(z)\dot{q}_i(t)|dzdt}{\int_{t=0}^{2\pi/\omega_i}\int_{z=0}^{L}\{N_i(z)\dot{q}_i(t)\}^2 dzdt} \quad (21)$$

In view of equation (20), equation (16) is re-expressed as

$$\ddot{q}_i + \omega_i^2 q_i - \frac{\kappa a cos(\Omega t)}{\bar{m}}\sum_j f_{ij}\, q_i + \mathrm{C}\omega_i\alpha_i\dot{q}_\iota = 0; (i,j = 1,2,3,\ldots.,N) \quad (22)$$

where C is the damping coefficient expressed as

$$\mathrm{C} = \frac{\rho D C_d}{2\bar{m}} N_{i,max} \quad (23)$$

Equation (22) yields the dynamic response of the riser when the external forces are ignored, thus, is considered appropriate for the stability analysis.

2.3 Floquet theory

The stability analysis applies the Floquet theory. The governing differential equation for every normal mode is written in state-space format using the following coordinate transformation:

$$\begin{cases} y_j = q_j(t) \\ y_{N+j} = \dot{q}_j(t) \end{cases} \quad (j = 1,2,\ldots,2N) \quad (24)$$

where N is the degree of freedom of the governing equation of motion. The specific value of N is determined for a given range of the excitation parameters. Equation (22) when expanded for every normal mode gives

$$\begin{Bmatrix} \dot{y}_1 \\ \dots \\ \dot{y}_N \\ \dot{y}_{N+1} \\ \dots \\ \dot{y}_{2N} \end{Bmatrix} = \begin{bmatrix} 0 & \dots & 0 & 1 & \dots & 0 \\ \dots & \dots & \dots & \dots & \dots & \dots \\ 0 & \dots & 0 & 0 & \dots & 1 \\ -\omega_1^2 + \dfrac{\kappa a \cos(\Omega t)}{\bar{m}} f_{1,1} & \dots & \dfrac{\kappa a \cos(\Omega t)}{\bar{m}} f_{1,N} & -\mathrm{C}\omega_1\alpha_1 & \dots & 0 \\ \dots & \dots & \dots & \dots & \dots & \dots \\ \dfrac{\kappa a \cos(\Omega t)}{\bar{m}} f_{N,1} & \dots & -\omega_N^2 + \dfrac{\kappa a \cos(\Omega t)}{\bar{m}} f_{N,N} & 0 & \dots & -\mathrm{C}\omega_N\alpha_N \end{bmatrix} \begin{Bmatrix} y_1 \\ \dots \\ y_N \\ y_{N+1} \\ \dots \\ y_{NN} \end{Bmatrix}$$

(25)

Equation is (25) is presented in compact form as

$$\dot{\boldsymbol{Y}} = \boldsymbol{A}(t)\boldsymbol{Y} \qquad (26)$$

where $\dot{\boldsymbol{Y}} = [\dot{y}_1, \dot{y}_2, \dots, \dot{y}_{2N}]^T$: $\boldsymbol{A}(t) = \boldsymbol{A}\left(t + \frac{2\pi}{\Omega}\right)$ is a $2N \times 2N$ periodic matrix and $\boldsymbol{Y} = [y_1, y_2, \dots, y_{2N}]^{\boldsymbol{T}}$.

Let $\boldsymbol{\phi}(t, 0)$ be the state transition matrix of equation (25). At an arbitrarily chosen time we can write

$$\dot{\boldsymbol{\phi}}(t, 0) = \boldsymbol{B}(t)\boldsymbol{\phi}(t, 0), \qquad t_0 = 0 \qquad (27)$$

At the end of one period, $\boldsymbol{\phi}(T, 0)$ is computed numerically by integrating the matrix differential equations over one period, $T = \frac{2\pi}{\Omega}$ with the initial condition $\boldsymbol{\phi}(0,0) = I_j$. If one of the eigenvalues of $\boldsymbol{\phi}(T, 0) > 1$, then the riser is unstable.

When the platform heave frequency and the natural frequency of the riser satisfy a certain relationship, the riser generates a parametric resonance. The riser mode directly determines the mode-coupling coefficient and the mode-dependent coefficient. The natural vibration characteristics of the riser are closely related to parametric vibration. Small displacement at the top of the riser has negligible effect on the linear stability characteristics, hence, the riser may be considered to be hinged at both ends; so that

$$y(z,t)|_{z=0} = 0, \left.\frac{\partial^2 y(z,t)}{\partial z^2}\right|_{z=0} = 0;\ y(z,t)|_{z=L} = 0, \left.\frac{\partial^2 y(z,t)}{\partial z^2}\right|_{z=L} = 0 \qquad (28)$$

Equation (28) defines the boundary condition of the problem.

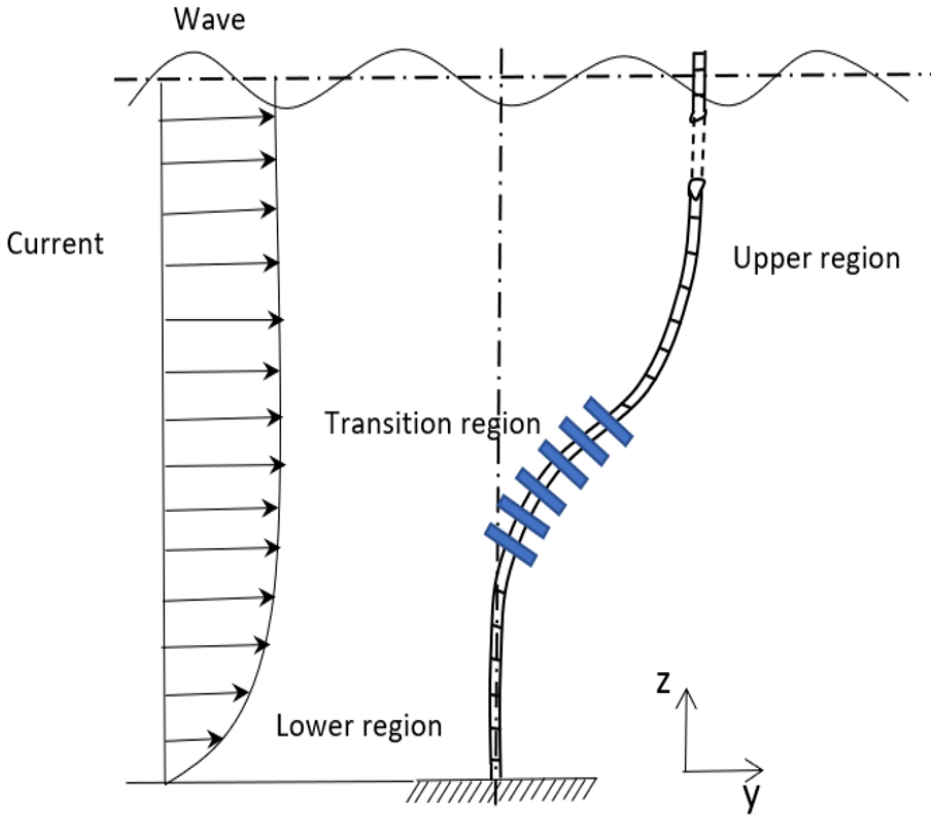

Figure 2: Element and node description of a CVAR

Table 1: Fixed parameters of the CVAR (Lou, Hu, et al., 2019)

Riser property	Symbol	Value
Outside diameter	D	0.3m
Wall thickness	WT	0.038
Water depth	zL	2438m
Elastic modulus	E	2.07×10^{11}Pa
Added mass coefficient	C_a	1
Drag coefficient	C_d	1
Material density	ρ_m	7850kg/m^3
Seawater density	ρ_w	1025 kg/m^3
Density of internal fluid	ρ_f	800 kg/m^3
Acceleration due to gravity	g	9.807m/s^2
Equilibrium hang-off tension, kN	$T_{t,eq}$	3700
Equilibrium tension at TDP, kN	$T_{TDP,eq}$	2500

Table 2: Section design of the CVAR (Lou, Hu, et al., 2019)

Section	Value

Lower region	Riser length	490 m
	Buoyancy block	300 - 490
	Buoyancy Factor	6
Transition region	Riser length	416 m
	Buoyancy block	490 - 907
	Buoyancy Factor	2
Upper region	Riser length	1695 m
	Buoyancy block	908 - 996
	Buoyancy Factor	-1.5

Results and discussion

Mesh sensitivity analysis/model validation

To determine an appropriate order of discretization (N) of the riser required to achieve a credible results, the riser system is initially assumed to exhibit free-vibration in single-mode $(i.e.\ f_{ij} = 0,\ i \neq j)$ with constant riser tension, $T(= T_{t,eq})$ at no damping condition $(C = 0)$. The results obtained for trial values of N = 4, N = 8 and N = 12 are presented as stability charts in Figure 3(a), Figure 3(c) and Figure 3(b) respectively. No significant difference is witnessed between the results of case N = 8 and that of N = 12, indicating that the CVAR is adequately described by the 8DOF system. Thus, the following analyses assume N to be equal to eight (8) to minimize computational difficulties. To validate the present solution program, similar result reported by Lou et al. (2019) is presented in Figure 3(d) and compared with that of the present study obtained at the same riser configuration shown in Figure 3(c).

(a) (b)

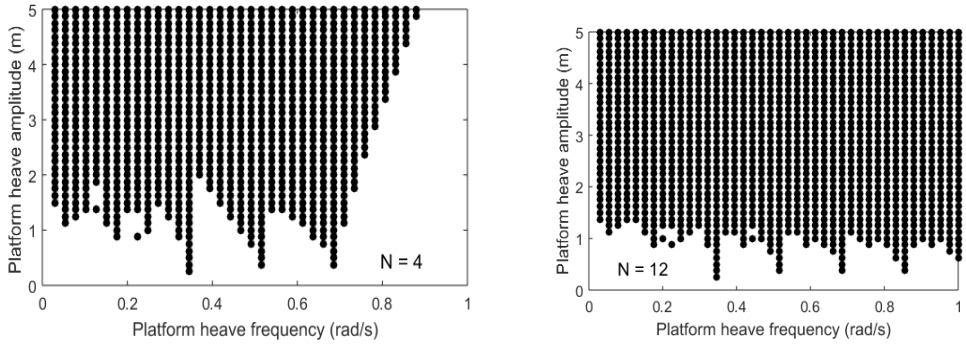

(c) (d)

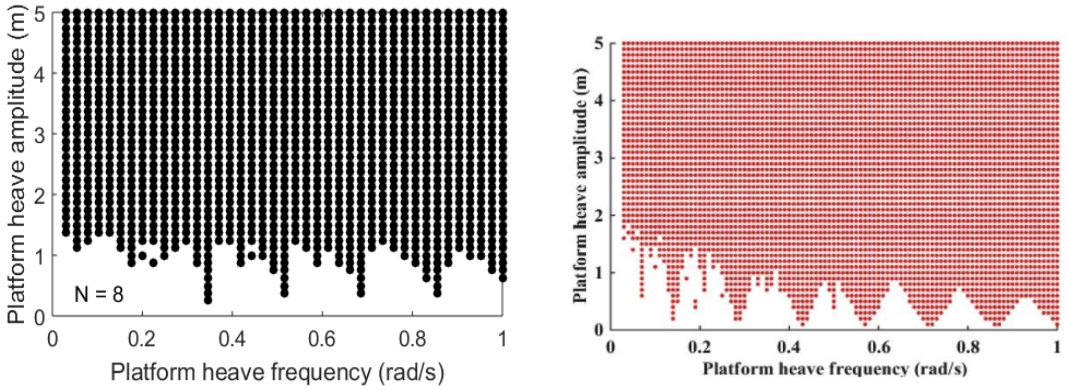

Figure 3: Stability chart of the CVAR at non-coupling, no-damping condition, considered as: (a) 4 DOF (b) 12 DOF and (c) 8 DOF, compared with (d) the result of Lou et al. (2019)

(a) (b)

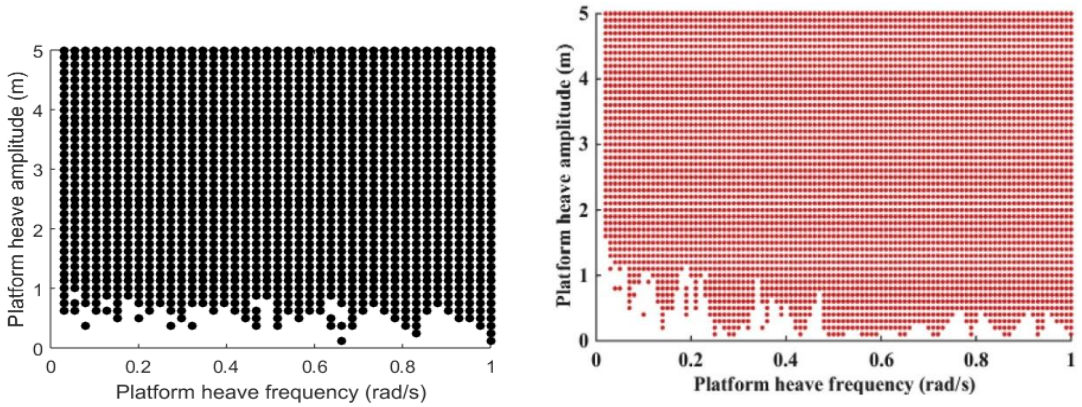

Figure 4: Stability chart of the CVAR at (a) no-damping condition, compared with (b) that of Lou et al. (2019) obtained at the same riser configuration

Further validation is carried out using results of the same CVAR system operated under mode coupling condition as shown in Figure 4. From the percentage overlap between the image of Figure 4(a) and that of Figure 4(b), about 95% overall similarity is observed between the results of the two-independent researches, suggesting that the present solutions show a reasonable agreement with related ones earlier reported in literature.

In either case, only marginal stability is seen at low amplitude heave for the nominal system. The first and the second-order unstable regions are excited. As the amplitude of the platform motion increases, higher-order unstable regions are activated. The results conform with the parametric resonance law which defines the condition for parametric resonance as (Brugmans, 2005):

$$\Omega = \frac{2\omega_i}{\lambda} \ (\lambda = 1,2,3, \ldots\ldots) \qquad (29)$$

where λ represents the order of riser instability.

(a) (b)

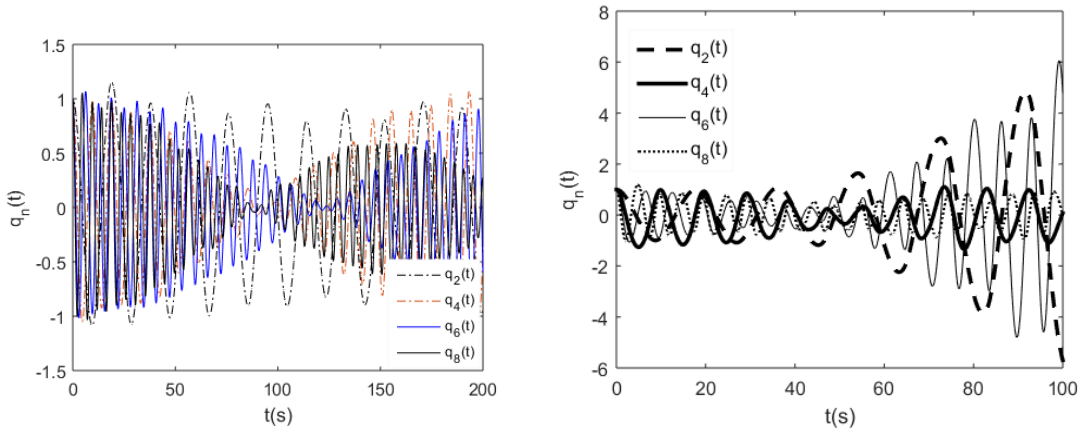

Figure 5: Time histories of the modal displacements obtained at (a) stable region where $a = 0.2, \Omega = 0.5, C = 0, T_t = T_{t,eq}$and (b) unstable region where $a = 0.5, \Omega = 2\omega_2, C = 0, T_t = T_{t,eq}$

The time histories of the modal displacements obtained for case 1: $(a = 0.2, \Omega = 0.5, C = 0, T_t = T_{t,eq})$ and case 2: $(a = 0.5, \Omega = 2\omega_2, C = 0, T_t = T_{t,eq})$ are presented in Figure 5(a) and Figure 5(b) respectively. In case 1, the vibration response confirms the system is marginally stable. The selected pair of the excitation parameter values $(a = 0.2, \Omega = 0.5)$ is located close to the imaginary line separating the stable and the unstable regions. Case 2 is a case where $\lambda = 1$, the second modal displacement, $q_2(t)$ lies on the first-order unstable region, thus, $q_2(t)$ and $q_6(t)$ are excited after 50 seconds of the observation as shown in Figure 5(b).

Improving stability characteristics of the CVAR system

The stability characteristics of the riser can be improved by modifying the riser damping or axial tension. The effects of damping on stability of the CVAR has been reported by Lou et al. (2019). Nevertheless, the present study noted that for the CVAR system operated under mode coupling, it could be very difficult, in practice, to achieve a desirable stability performance for the CVAR system, by mere adjusting the damping coefficient. The effects of increased axial tension on stability of the CVAR operated under mode coupling (at no-damping) condition is analysed in the present study. Figure 6(a) and Figure 6(b) are the stability charts of the risers when the hang-off tension is increased from the static equilibrium condition($T_{t,eq}$) to $1.5T_{t,eq}$ and $2T_{t,eq}$ respectively. The effects of increased axial tension are that of widening the stable sub-regions found in the low amplitude zone, and increasing the critical amplitude at which the system becomes unstable. However, it does not

eliminate undue excitations within the first-order and the second-order unstable regions.

(a) (b)

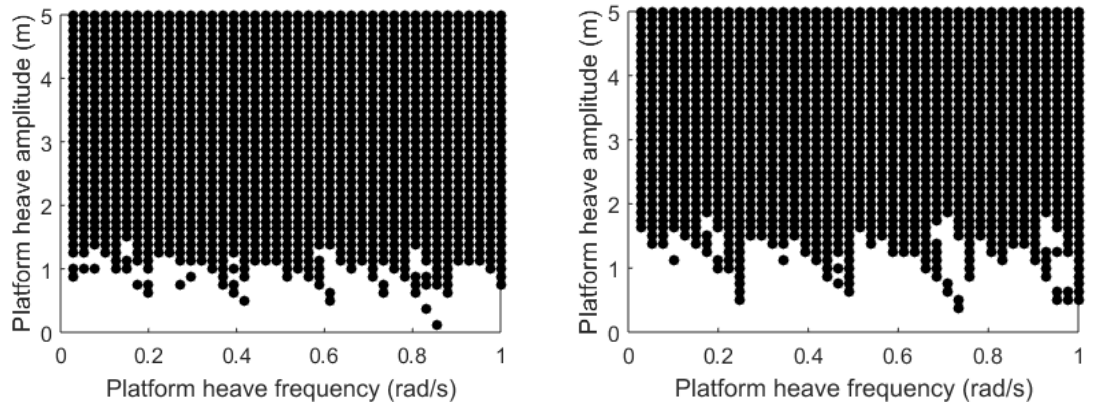

Figure 6: Stability chart for the CVAR system showing the effects of increasing riser tension from $T_{t,eq}$ to (a) $1.5T_{t,eq}$ and (b) $2T_{t,eq}$

(a) (b)

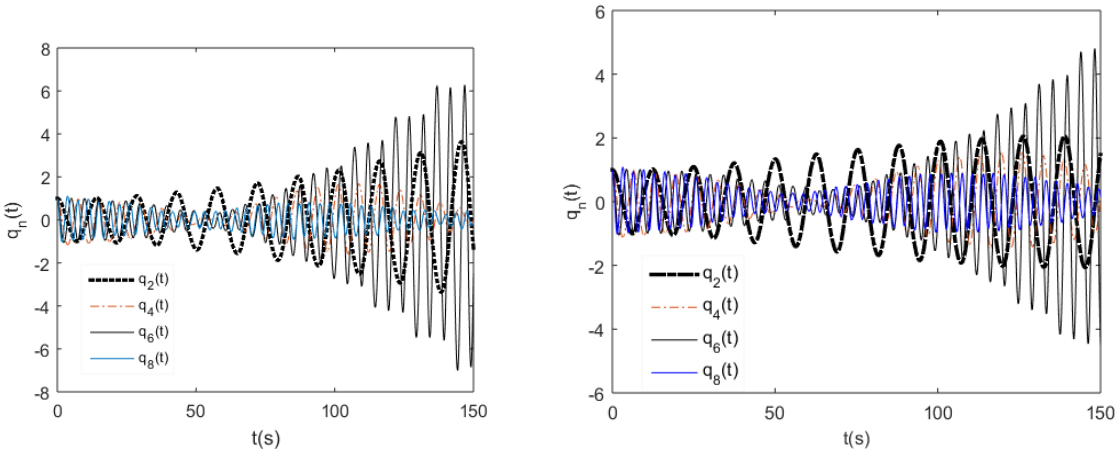

Figure 7: Time histories of the modal displacements obtained at: (a) $a = 0.5, \Omega = 2\omega_2, C = 0, T_t = 1.5T_{t,eq}$ and (b) $a = 0.5, \Omega = 2\omega_2, C = 0, T_t = 2T_{t,eq}$

The vibration response of the CVAR system operated at the first-order unstable region of the second modal displacement with $T_t = 1.5T_{t,eq}$ and $T_t = 2T_{t,eq}$ are shown in Figure 7(a) and Figure 7(b) respectively. With the value of T_t set to $1.5T_{t,eq}$, the second and sixth displacement modes became unstable within 150 seconds of the observation, while the fourth and eight displacement modes are still at marginal stability. When the value of T_t is increased further to $2T_{t,eq}$, the amplitudes of vibration of the unstable modes including $q_2(t)$ and $q_6(t)$ are significantly reduced, suggesting that degrees of instability of the affected regions

are substantially reduced. However, the excitations at the first-order unstable region are not readily eliminated by increasing the riser tension alone.

When the added tension is removed, and damping coefficients of value C = 0.1, C = 0.3, C = 0.5 and C = 0.8 are set for the CVAR system, the resulting stability charts are shown in Figure 8(a), Figure 8(b), Figure 8(c) and Figure 8(d) respectively. The effects of increased damping in the range of $C \leq 0.1$ increased the critical platform heave amplitude, a_*, from a value $\leq 0.5m$ to a value $\geq 1m$, and eliminate the undue excitations at the first-order and second-order unstable regions as shown in Figure 8(a). The corresponding modal displacement histories obtained at $\Omega = 2\omega_2$ to illustrate the damping effect is shown in Figure 9(a) When the damping coefficient is increased further from 0.1 up to 0.8, the effects appear less significant towards lower platform heave frequency as highlighted in Figure 8(b) to Figure 8(d). The modal displacement histories obtained at $\Omega = 2\omega_2$ to account for the effects of increased damping is shown in Figure 9(b)

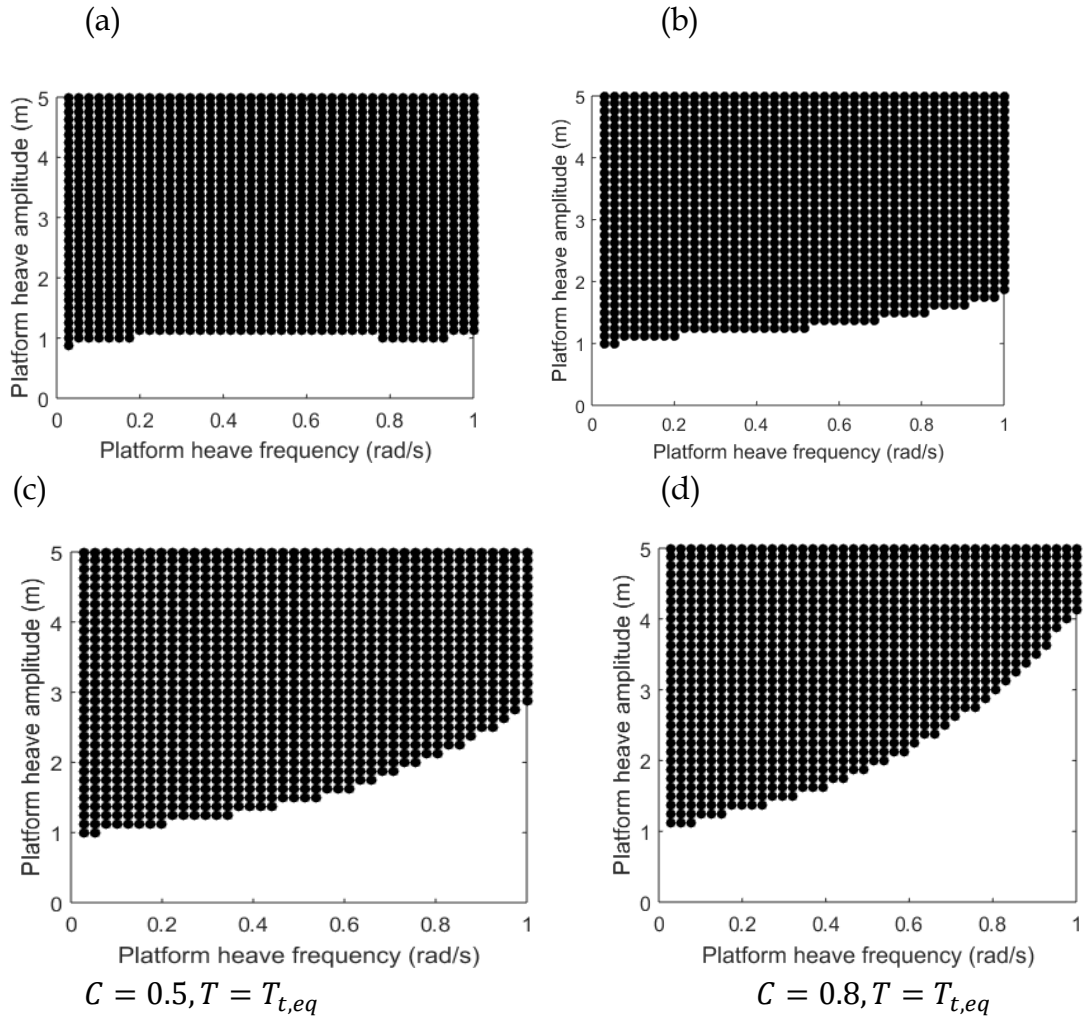

Figure 8: Stability charts for the CVAR system showing the effects of hydrodynamic damping, C at: (a) $C = 0.1$, (b) $C = 0.3$, (c) $C = 0.5$ and (d) $C = 0.8$

(a) (b)

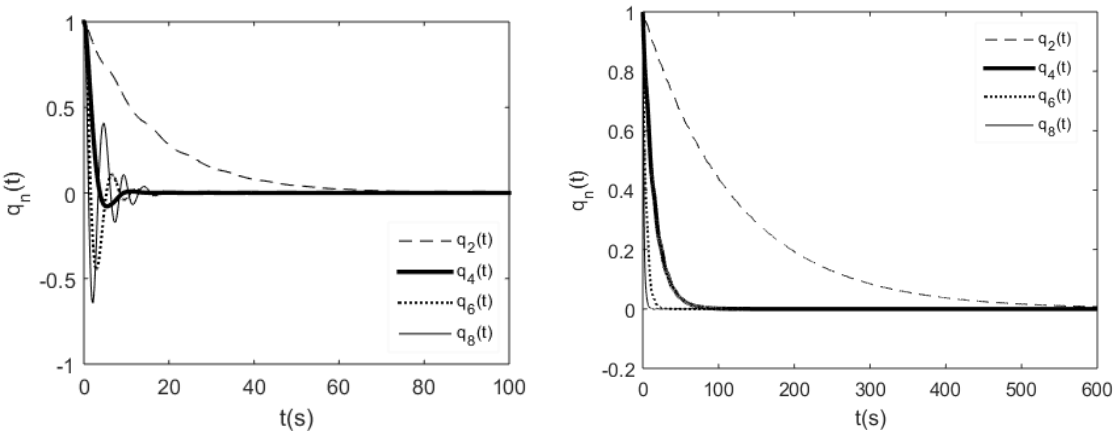

Figure 9: Time histories of the modal displacements obtained at: (a) $a = 0.5, \Omega = 2\omega_2, C = 0.1, T_t = T_{t,eq}$ and (b) $a = 0.5, \Omega = 2\omega_2, C = 0.8, T_t = T_{t,eq}$

(a) (b)

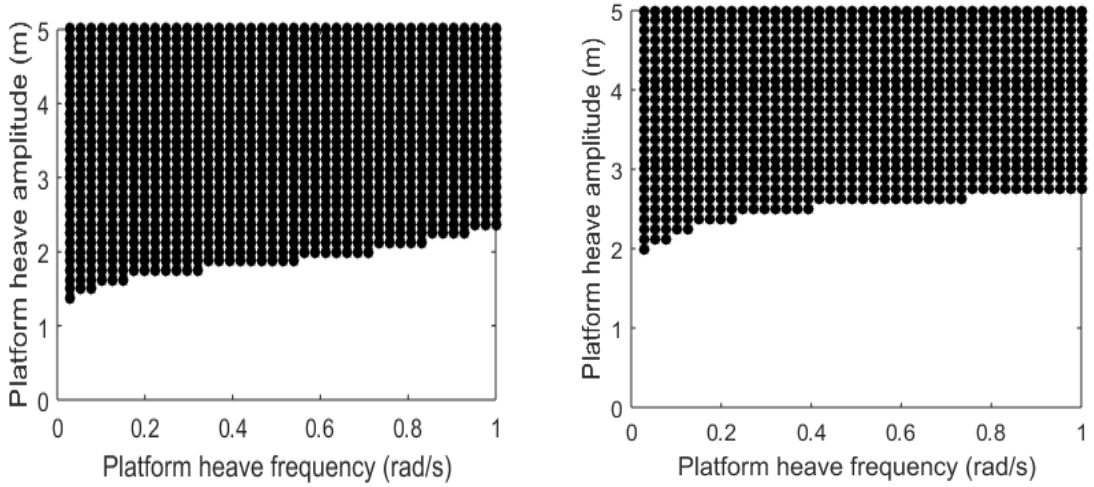

Figure 10: Stability chart for the coupled CVAR System showing the combined effects of increased hang-off tension at (a) $T_t = 1.5T_{t,eq}$ and (b) $T_t = 2T_{t,eq}$, assuming $C = 0.5$ in each case

Improvements in stability favouring higher platform heave frequencies combined with higher platform heave amplitude associated with increased damping coefficient is of less practical importance since high frequency platform heave motions usually occur with relatively low amplitude, and vice versa. In other words, to take full advantage of the damping effect, the trend must be reversed. One practical approach to achieve this is to harmonize the effects of increased riser axial tension and damping. Figure 10(a) and Figure 10(b) show the combined effects of increasing hang-off tension from the equilibrium state, $T_{t,eq}$ to $2T_{t,eq}$ at steps of

$0.5T_{t,eq}$ on the stability of the CVAR system, assuming the damping coefficient is 0.5. Evidently, stability is compelled to improve towards the low frequency – high amplitude region, in line with the basic field requirement, by increasing the riser tension simultaneously with the damping coefficient. A hundred percent (100%) increase in tension, relative to the static equilibrium condition or more is required of the underdamped system (@ C = 0.5) to increase the critical heave amplitude from the nominal value of $a_* \geq 1m$ to a value $a_* \geq 2m$, which is expected to satisfy most field requirements, [see Figure 10(b)].

To validate the stability charts of Figure 10 which account for the synchronized effects of the riser tension and damping, a combination of the excitation parameter values which lie clearly in the unstable domain such as: $a = 3, \Omega = 2\omega_2$, is first considered. The vibration response of the damped system observed at this instance is compared when the hang-off tension, T_t, is set at $1.5T_{t,eq}$ and $2T_{t,eq}$ in Figure 11(a) and Figure 11(b). The results suggest that due to high level of instability, it is not possible to stabilize the riser operated in this parameter space at damping coefficient of 0.5, even with 100% increase in the axial tension. However, the amplitude of vibration or the degree of instability of the riser decreased proportionally to the increase in tension.

(a) (b)

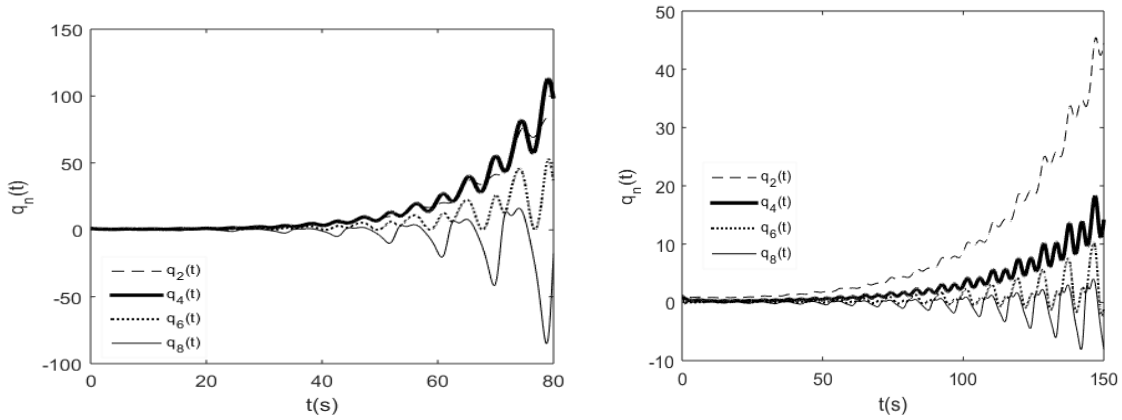

Figure 11: Time histories of the modal displacements obtained at a region where (a) $a = 3, \Omega = 2\omega_2, C = 0.5, T_t = 1.5T_{t,eq}$ and (b) $a = 3, \Omega = 2\omega_2, C = 0.5, T_t = 2T_{t,eq}$

(a) (b)

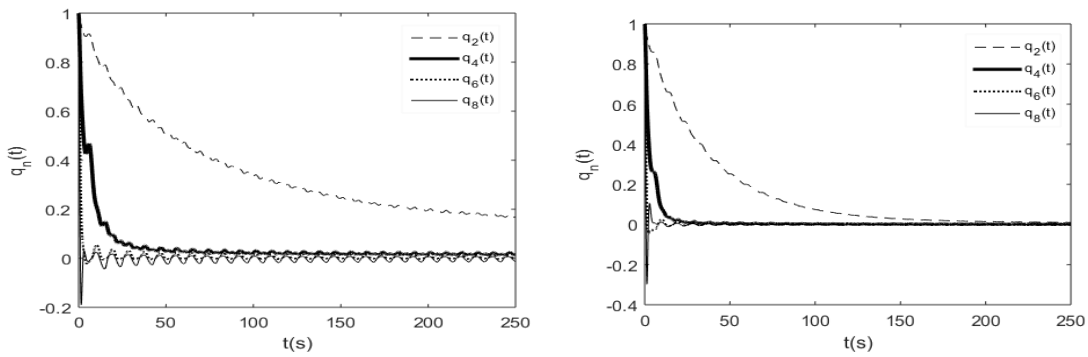

Figure 12: Time histories of the modal displacements obtained at (a) region where $a = 2, \Omega = 2\omega_2, C = 0.5, T_t = 2T_{t,eq}$ and (b) unstable region where $a = 2, \Omega = 2\omega_2, C = 0.5, T_t = 2T_{t,eq}$

Conclusion

The conclusion arrived at in this study are:

(i) The CVAR system excited at nominal state (i.e. without added tension or damping) by the platform heave motion in a frequency range < 1rad/sec. is marginally stable. The critical platform heave amplitude is $\leq 0.5m$.

(ii) The excitation frequency and amplitude have considerable effects on the stability characteristics of the CVAR system which can be controlled by adjusting the riser tension or the damping to alter the riser natural frequency

(iii) When the axial tension alone is increased from its static equilibrium value, the stable sub-regions in the parameter space is enlarged proportionally to the amount of tension added over the entire frequency range, leading to a corresponding increase in the critical platform heave amplitude. However, this does not eliminate undue excitation at the first-order unstable regions.

(iv) When the added tension is removed and damping applied, stability of the CVAR system also improves according to the level of damping. However, the damping effect apparently favours the region of high heave frequencies combined with high heave amplitude, which is of less practical importance since high frequency platform motion naturally occurs with relatively low amplitude

(v) Holistic improvement in stability of the CVAR system over the entire design space is seen when the damping effects are harmonized with the effects of increased hang-off tension

(vi) This study found that for a fairly damped CVAR system of damping coefficient C = 0.5, about 100% increase in the hang-off tension from the equilibrium state is required to obtain a desirable minimum critical

platform heave amplitude of 2m, which is expected to satisfy most field requirements

(vii) Any solution that satisfies specific field requirements must be matched with the capacity of the available production facilities

Bibliography

Ağbulut, M., & Sarıdemir, S. (2021). A general view to converting fossil fuels to cleaner energy source by adding nanoparticles. , *2021*, *42*(13). https://doi.org/10.1080/01430750.2018.1563822

American Oil and Gas Reporter. (2025). *Statistical Review of World Energy*.

Bai, Y., & Bai, Q. (2019). Subsea Production Risers. In *Subsea Engineering Handbook* (Second Edi).

Bakis, K. N., & Srinil, N. (2019). Internal Flow-Induced Instability Analysis of Catenary Risers Marine 2019. *VIII International Conference on Computational Methods in Marine Engineering MARINE 2019*, 525–536.

Brugmans, J. (2005). *Parametric Instability of Deep-Water Risers. Tu Delft Faculty of Civil Engineering & Geosciences Hydraulic Engineering.*

Buberg, T. (2014). *Design and Analysis of Steel Catenary Riser Systems for Deep Waters* (Issue June). Norwegian University of Science and Technology.

C, A. S. M., L, S. C., & R, S. A. (2024). Petroleum exploration and production in Brazil : From onshore to ultra-deepwaters. *Petroleum Exploration and Development*, *51*(4), 912–924. https://doi.org/10.1016/S1876-3804(24)60515-X

Gonzalez, G. M., De Sousa, J. R. M., & Sagrilo, L. V. S. (2015). An Unbonded Flexible Pipe Finite Element Model. *Proceedings of the XXXVI Iberian Latin American Congress on Computational Methods in Engineering*, *April 2016*. https://doi.org/10.20906/cps/cilamce2015-0373

Khan, R. A., Kaur, A., Singh, S. P., & Ahmad, S. (2011). Nonlinear dynamic analysis of marine risers under random loads for deepwater fields in Indian offshore. *Procedia Engineering*, *14*, 1334–1342. https://doi.org/10.1016/j.proeng.2011.07.168

Lei, S., & Zheng, X. (2016). Numerical analysis of the effects of parametric excitation on riser VIV. *Proceedings of the ASME 35th International Conference on Ocean, Offshore and Arctic Engineering, Vol. 2, Busan, South Korea June, Pp. 39–49. New York: American Society of Mechanical Engineers.*, 19–24.

Li, F., Guo, H., Li, X., Liu, Z., Gu, H., & Cui, P. (2021). Parametric analyses of the dynamic response and fatigue life of a compliant vertical access riser with internal flow. *Journal of Marine Science and Technology (Taiwan)*, *29*(5), 638–651. https://doi.org/10.51400/2709-6998.2466

Liang, W., Lou, M., Wang, Y., & Zhang, R. (2023). Dynamic Analysis of A Deep-Water Compliant Vertical Access Riser with A Variable Length During

Installation. *China Ocean Engineering*, *37*, 568–579. https://doi.org/10.1007/s13344-023-0048-9

Liu, X. Q., Xiang, H., Meng, S., Yu, R., Qiu, N., Wei, Y., Fu, L., Liu, L., & Ming, G. (2020). Mechanical analysis of deepwater drilling riser system based on multibody system dynamics. *Petroleum Science*, *0123456789*. https://doi.org/10.1007/s12182-020-00506-1

Lou, M., Hu, P., Qi, X., & Li, H. (2019). Stability analysis of deepwater compliant vertical access riser about parametric excitation. *International Journal of Naval Architecture and Ocean Engineering*, *11*(2), 688–698. https://doi.org/10.1016/j.ijnaoe.2019.02.005

Lou, M., Li, R., Wu, W., & Chen, Z. (2019). Static performance analysis of deepwater compliant vertical access risers. *International Journal of Naval Architecture and Ocean Engineering*, *11*(2), 970–979. https://doi.org/10.1016/j.ijnaoe.2019.04.007

Vandiver, J. ., & Li, L. (2005). *SHEAR7 V4.4 Program Theoretical Manual*.

Woo, N. S., Han, S. M., & Kim, Y. J. (2016). Design of a marine drilling riser for the deepwater environment. *WIT Transactions on Engineering Sciences*, *105*(Afm). https://doi.org/10.2495/AFM160201

Wu, Z., Xie, C., Mei, G., & Dong, H. (2019). Dynamic analysis of parametrically excited marine riser under simultaneous stochastic waves and vortex. *Advances in Structural Engineering 2*, *22*(1), 268–283. https://doi.org/10.1177/1369433218783968

Zhu, Q. (2019). Developments on CO 2 -utilization technologies. *Clean Energy*, *3*(2), 85–100. https://doi.org/10.1093/ce/zkz008

Zuoqian, W., Zifei, F. A. N., Xingyang, Z., Baolei, L. I. U., & Xi, C. (2022). Status , trends and enlightenment of global oil and gas development in 2021. *Petroleum Exploration and Development*, *49*(5), 1210–1228. https://doi.org/10.1016/S1876-3804(22)60344-6